Kaposi's sarcoma–associated herpesvirus stably clusters its genomes across generations to maintain itself extrachromosomally

Kaposi's sarcoma–associated herpesvirus stably clusters its genomes across generations to maintain itself extrachromosomally

Ya-Fang Chiu,[1,2,4,5,6] Arthur U. Sugden,[7,8] Kathryn Fox,[1,3] Mitchell Hayes,[1] and Bill Sugden[1]

[1]McArdle Laboratory for Cancer Research, [2]Morgridge Institute for Research, and [3]Flow Cytometry Laboratory, Carbone Cancer Center, University of Wisconsin–Madison, Madison, WI
[4]Research Center for Emerging Viral Infections and [5]Department of Microbiology and Immunology, Chang-Gung University, Taoyuan, Taiwan
[6]Department of Medical Laboratory, Chang-Gung Memorial Hospital, Taoyuan, Taiwan
[7]Department of Neuroscience, Brown University, Providence, RI
[8]Beth Israel Deaconess Medical Center, Harvard Medical School, Boston, MA

Genetic elements that replicate extrachromosomally are rare in mammals; however, several human tumor viruses, including the papillomaviruses and the gammaherpesviruses, maintain their plasmid genomes by tethering them to cellular chromosomes. We have uncovered an unprecedented mechanism of viral replication: Kaposi's sarcoma–associated herpesvirus (KSHV) stably clusters its genomes across generations to maintain itself extrachromosomally. To identify and characterize this mechanism, we developed two complementary, independent approaches: live-cell imaging and a predictive computational model. The clustering of KSHV requires the viral protein, LANA1, to bind viral genomes to nucleosomes arrayed on both cellular and viral DNA. Clustering affects both viral partitioning and viral genome numbers of KSHV. The clustering of KSHV plasmids provides it with an effective evolutionary strategy to rapidly increase copy numbers of genomes per cell at the expense of the total numbers of cells infected.

Introduction

Multiple human tumor viruses, including the papillomaviruses, the gammaherpesviruses, Epstein–Barr virus (EBV), and Kaposi's sarcoma herpesvirus (KSHV), maintain their genomes as plasmids in proliferating cells. The viral genomes express only a few genes in the tumor cells and do not make progeny virus. One pivotal step for these viruses in tumor cells is the segregation of their plasmid genomes to daughter cells (Grundhoff and Ganem, 2004; Sugden, 2014). Examining this step in the life cycles of KSHV and EBV has allowed us to uncover its intrinsic biology and will aid in developing virus-specific, cancer-specific therapies for these tumor viruses.

Mammals use large, repetitious cis-acting centromeres and large, complex trans-acting kinetochores to segregate chromosomes faithfully to daughter cells (Nicklas, 1997). Gammaherpesviruses have evolved multiple strategies to exploit this cellular machinery to support maintenance of their genome in cells. They also provide selective advantages to the infected cells to ensure that cells that maintain their genomes outgrow those that lose them (Grundhoff and Ganem, 2004; Sugden, 2014). KSHV and EBV both encode cis-acting origins of DNA synthesis and trans-acting origin-binding proteins to mediate their synthesis and partitioning (Hammerschmidt and Sugden, 2013; Lieberman, 2013). Some features of EBV's exploitation of its host cell's segregation mechanism have been identified; EBV uses a discrete origin of DNA synthesis (DS), a separate maintenance element (FR), and the protein, EBNA1, which binds both elements for its plasmid synthesis (Chaudhuri et al., 2001; Dhar et al., 2001; Schepers et al., 2001). EBNA1 tethers EBV plasmids to chromosomal AT-rich DNA sequences directly to mediate quasi-faithful partitioning (Marechal et al., 1999; Sears et al., 2004; Nanbo et al., 2007; Hodin et al., 2013; Chakravorty and Sugden, 2015). Approximately 88% of its newly duplicated sister plasmids are bound to opposite sister chromatids during S phase and, as such, evenly divide between daughter cells (Nanbo et al., 2007). The related gammaherpesvirus KSHV differs profoundly from EBV. Detailed examinations have shown that the KSHV genome encodes 16 or more sets of replication origins, each located within a copy of its terminal repeats (TRs) and uses one viral protein, LANA1, to bind these origins and mediate their DNA synthesis (Ballestas et al., 1999; Cotter and Robertson, 1999; Ballestas and Kaye, 2001; Hu et al., 2002; Krithivas et al., 2002; Barbera et al., 2004; Ye

Correspondence to Bill Sugden: sugden@oncology.wisc.edu

Abbreviations used: CAPS, computer-assisted plasmid summation; EBV, Epstein–Barr virus; IRES, internal ribosomal entry site; KSHV, Kaposi's sarcoma–associated herpesvirus; SIM, structured illumination microscopy; TR, terminal repeat.

The Rockefeller University Press
J. Cell Biol. Vol. 216 No. 9 2745–2758
https://doi.org/10.1083/jcb.201702013

et al., 2004; Shrestha and Sugden, 2014). LANA1 binds these replication origins directly but does not tether them directly to chromosomal DNA. Rather it tethers the KSHV genome to histones H2A and H2B in nucleosomes (Ballestas and Kaye, 2001; Barbera et al., 2006; Hellert et al., 2015).

We have examined KSHV to understand how the tethering of its genomes to nucleosomes via LANA1 mediates its segregation, an event essential to KSHV maintaining the tumors it causes. Quantitative FISH unexpectedly showed that the distribution of signals detected in primary effusion lymphoma (PEL) cells of KSHV genomes differs from that of EBV genomes: the distribution of KSHV signals was significantly broader than that of EBV signals. Live-cell imaging (Robinett et al., 1996) was combined with an independent, computational simulation to elucidate both this discrepancy and KSHV's unprecedented mode of segregation. KSHV tethers its genomes not only to nucleosome-bound chromosomal DNA but also to nucleosome-bound viral DNA to form clusters of genomes that partition as units. Superresolution structured illumination microscopy (SIM) shows that these clusters are coherent aggregates not resolvable into their constituent plasmids. We have uncovered the mechanism of cluster formation by examining substitutions of LANA1 with moieties from EBNA1, which show that nucleosome binding is essential for clustering. This cluster-forming mechanism confers a surprising distribution of plasmids in cells and an advantage to KSHV in establishing itself after infection that was first predicted by the simulation and then confirmed experimentally. Clustering, as predicted computationally and observed in live cells, leads to a rapid establishment of high viral copy numbers in a population of cells.

Results

Detecting EBV and KSHV genomes quantitatively by FISH

FISH was used to detect EBV and KSHV genomes in PEL cells. PELs are lymphomas associated with both viruses; all harbor KSHV and ∼90% also harbor EBV genomes, with the mean number of KSHV genomes per cell exceeding those of EBV (Cesarman et al., 1995; Carbone et al., 2010; Giffin and Damania, 2014). EBV genomes were assayed in BC-2 cells, which have both viruses, and KSHV genomes were assayed in BCBL-1 cells, which have only KSHV plasmids. FISH was rendered quantitative by measuring each signal with computer-assisted plasmid summation (CAPS; Chiu et al., 2013), a program that sums the intensities in each selected pixel of a CCD image in three dimensions and removes the background intensities measured in an annulus surrounding the signal in each *z*-plane. (CAPS is explained for users and available at http://caps.grapheasy.org). The number of KSHV signals per cell exceeded those of EBV as expected (Fig. 1, A and B). Both viruses also had signals with similar, low intensities likely reflecting single plasmids; however, the intensities of KSHV signals extended unexpectedly to 10 times those of its lower values, whereas those of EBV did not (Fig. 1 C).

Visualizing KSHV genomes reveals their clustering and unequal partitioning

We applied fluorescent tagging of KSHV genomes in live cells to track individual plasmids as they duplicate and partition to daughter cells to understand the findings with quantitative FISH.

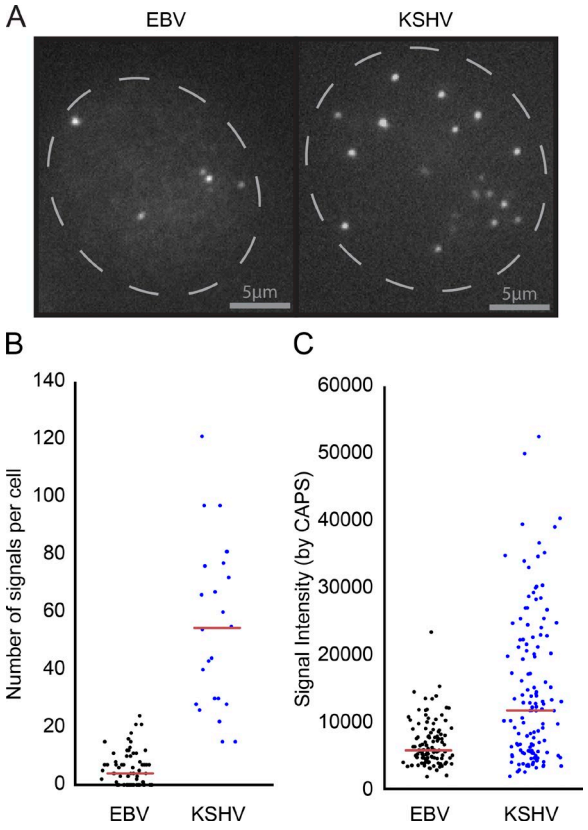

Figure 1. **Quantitative FISH of EBV and KSHV in PEL cells.** (A) Example of a BC-2 cell assayed for EBV and a BCBL-1 cell assayed for KSHV by FISH. Shown is a single 0.35-µm *z*-plane of cells with signals detected by probes to EBV or KSHV. The intensities of raw signals were measured and summed in four to seven *z*-planes with CAPS. (B) The number of KSHV signals exceeded that of EBV measured in BC-2 cells (EBV, $n = 66$; KSHV, $n = 24$). (C) The signals of lower intensities were similar for both viruses; those of KSHV, however, extended to 10-fold higher values. The red lines indicate the medians for each of the distributions (EBV, $n = 111$; KSHV, 131). The two distributions in C differ as determined by the Kolmogorov–Smirnov test ($P = 2.3 \times 10^{-5}$).

A derivative of KSHV, KLacO, was engineered to express resistance to hygromycin B and contain ∼250 copies of the Lactose operator *LacO* (Fig. 2). It was stably introduced into the SLK epithelial cell line, which expressed the Lac repressor fused to tdTomato red fluorescent protein (LacI/tdTomato). We followed the signals of tagged KSHV genomes that were dependent on the binding of LacI/tdTomato; imaging the cells in the presence of IPTG eliminated them. Three tests demonstrated that KLacO is maintained and replicated similarly to wild-type KSHV. First, the KLacO plasmids were maintained extrachromosomally, as measured in Gardella gels (Norby et al., 2012), which can discriminate between integrated and extrachromosomal DNAs (Gardella et al., 1984). Second, they replicated in a licensed manner, as determined by density-shift experiments (Fig. S1, A and B). Third, the proliferation of cells with or without KLacO was identical in the absence of selection, indicating that the viability of the host cells was unaffected by the viral genome (Fig. S1, C and D).

Clones of SLK cells carrying KLacO were imaged in an epifluorescence microscope, and their viral genomes were visualized as punctate fluorescent signals over time. These signals differed dramatically from those previously observed in studies of EBV plasmids by live-cell imaging (Nanbo et al., 2007; Chiu

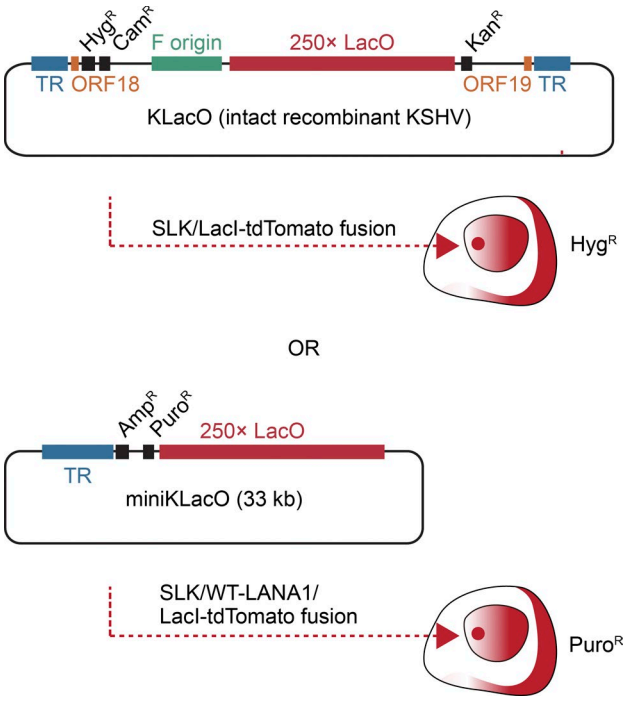

Figure 2. **Map of KSHV derivatives KLacO and miniKLacO.** KLacO is an infectious derivative of BAC36 that has ~250 binding sites for the Lac repressor. miniKLacO has these sites and 16 copies of KSHV's TRs.

et al., 2013). The intensities of individual EBV puncta varied only by a few fold within a latently infected cell (as shown in Fig. 8 B), and these puncta were demonstrated to be individual plasmids. Only in cells supporting the viral productive cycle did they increase by 20- to 30-fold (Chiu et al., 2013). In contrast, some punctate signals derived from KLacO early in G1 varied in their intensities 10-fold or more, whereas other signals were observed to dissociate into multiple daughters with decreased intensities (Fig. 3 A, d and e; and Video 1 A). These differences in intensities did not result from differing numbers of *LacO* repeats in the KLacO genomes (Norby et al., 2012) and therefore arose from high, local concentrations of KLacO plasmids that we term clusters. We determined also that polymers of *LacO* do not yield clusters when present in EBV plasmids or when integrated (Fig. 8 B and Fig. S1 E, a). We followed >800 fluorescent signals from KLacO in 105 mitotic cells to characterize their partitioning. Only 13% of the daughter cells received equal numbers of signals, and in these cases, the sum of the intensities of their signals often differed (Fig. 3 A and Table S1). These measurements demonstrate that KLacO partitions unequally to daughter cells.

Identifying the viral factors needed for KSHV plasmids to cluster

KLacO is an intact derivative of the BAC36 version of KSHV (Zhou et al., 2002; Norby et al., 2012). It encodes the viral genes that support productive infection or can act as oncogenes (Gao et al., 1997; Thome et al., 1997; Bais et al., 1998; Lee et al., 1998; Muralidhar et al., 1998; Ojala et al., 1999; Guasparri et al., 2004; Samols et al., 2007; Wies et al., 2008; Santag et al., 2013; Giffin and Damania, 2014). To test whether the observed clustering of KLacO plasmids is a result solely of the known cis and trans elements of KSHV's plasmid replicon, we developed miniKLacO (Fig. 2). MiniKLacO contains only origins of replication located in the TRs, drug resistance to puromycin, and *LacO* binding sites for fluorescent tracking. MiniKLacO contains 16 copies of the TRs, which we have found to be the minimal number needed for wild-type maintenance of these viral plasmids (Shrestha and Sugden, 2014). MiniKLacO was introduced into SLK cells expressing LacI/tdTomato fusions and LANA1, the only trans-acting viral factor required for plasmid maintenance (Ballestas et al., 1999; Ye et al., 2004).

MiniKLacO behaved as did KLacO; it was maintained extrachromosomally and intact as shown in Gardella gels and Southern blots. Importantly, signals from miniKLacO were observed in live cells to form high local concentrations or clusters (Fig. 3 B). These signals represented clusters of plasmids, as they were observed sometimes to dissociate and also to grow at least eightfold in intensity over multiple generations (Fig. 3 B, c and d, f–i, and n and o; and Video 1 A). Importantly, the signals on dissociating can move apart consistently with their being distinct smaller clusters of plasmids rather than plasmids tethered along a chromosome. The TR in cis and LANA1 in trans are thus the only elements of KSHV necessary to form clusters of viral plasmids. We used SIM with live cells to analyze the structure of clusters of KSHV plasmids. SIM showed that clusters could not be separated into smaller constituents over a sixfold range of intensities, as measured with CAPS (Fig. 4 A, a–c; and Video 2). Some of the largest analyzed clusters were irregular in shape (Fig. 4 A, e; and Video 2), perhaps reflecting their recent formation or imminent dissociation.

KSHV clusters its genomes in PEL cells

We used a second approach to verify the presence of clusters of KSHV genomes in the dually infected PEL tumor-derived cell lines, BC-1 and BC-2. The numbers of KSHV and EBV genomes in them were measured by FISH and quantitative PCR in the same cell populations for each cell line. The number of viral genomes was quantified with probes specific to each virus and normalized to the levels of the cellular *Rhodopsin* gene. In this experiment, measurements of the number of copies of EBV served as an internal control in the same cells and showed that the EBV genomes were detected equally by both assays and thus are unclustered (Fig. 4 B). In the same cells, 30% more KSHV genomes were detected with PCR than with FISH, demonstrating that KSHV plasmids are clustered in PEL cells (Fig. 4 B). These findings show that wild-type KSHV genomes do cluster as also illustrated in Fig. 1, indicating that clustering is not a result of engineered derivatives of KSHV.

Clusters of KSHV plasmids participate in synthesis and partitioning

The plasmids within clusters appeared not to be synthesized simultaneously and could dissociate through much of the cell cycle (Fig. 3, A and B). This dynamic nature of the observed fluorescent signals precluded measuring a synchronous doubling of their intensities during S phase. However, if clusters of KSHV plasmids are synthesized as expected from density-shift experiments (Fig. S1, A and B), then the sum of intensities of the signals derived from miniKLacO, for example, should on average double during S phase. We measured the intensities of signals of miniKLacO from the beginning of G1 hourly through G2 for 24 cells and found that those extrachromosomal plasmids doubled as expected by the end of S phase (Fig. 5 A). We also measured the intensities of a signal from an integrated

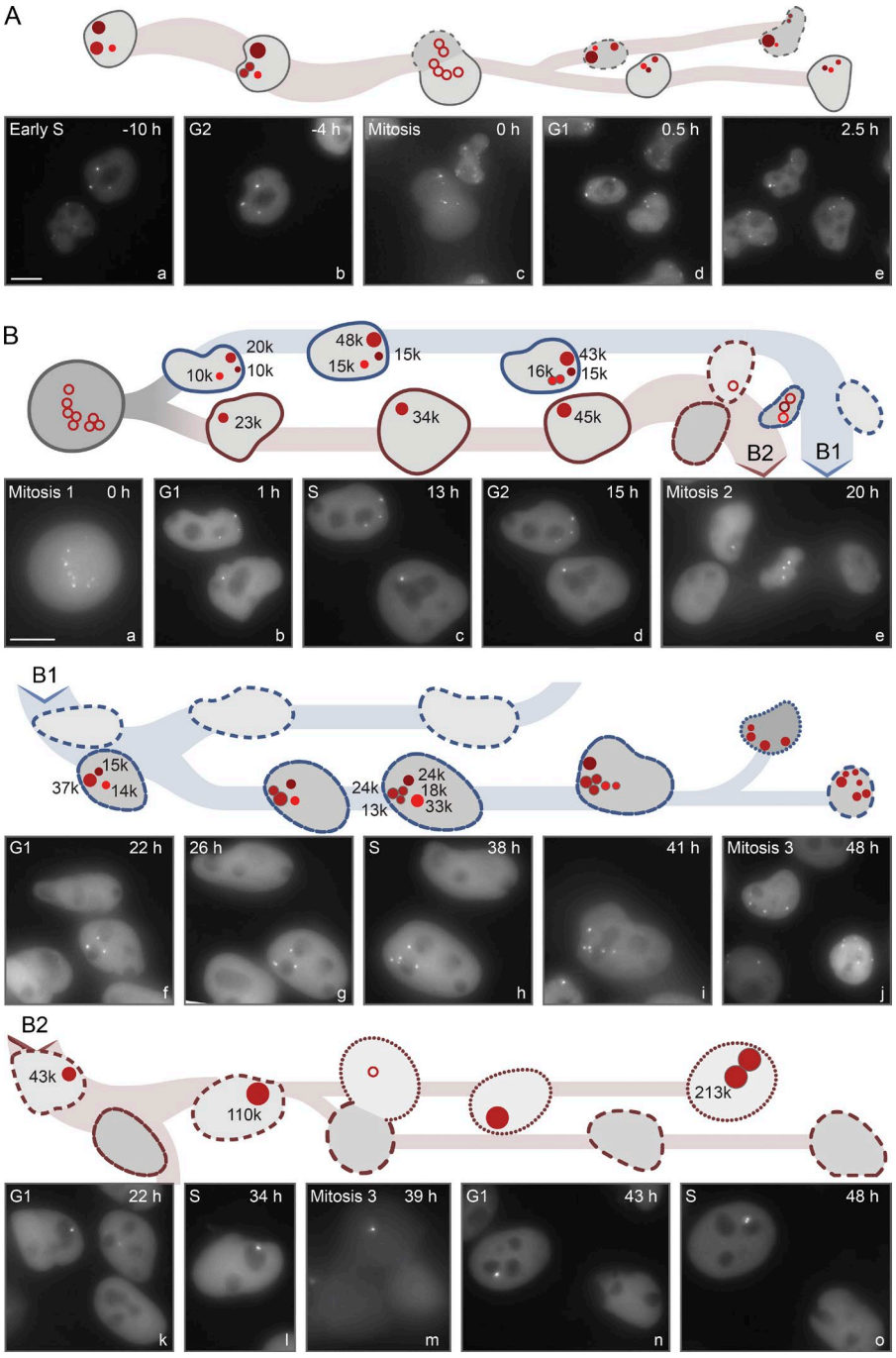

Figure 3. **Time-lapse analysis of KLacO and miniKLacO in live cells.** (A) Live-cell images illustrating clusters of KLacO plasmids and their segregation during mitosis. KLacO signals in SLK cells expressing the LacI-tdTomato fusion were followed over a 60-h period for at least two generations. Cartoons above the images depict the imaged cells with their intensities (a.u.) approximated by the diameters of the signals in the cartoons. Intensities cannot be measured reliably in mitosis, so these signals are unfilled in the cartoon. A given cell and its progeny are identified by having related outlines. A representative example is shown in which images from multiple *z*-planes are compressed: signals in the parental cell (a) differ in their intensities; one signal dissociates into two signals (b) with lower intensities before mitosis (c); each daughter cell receives three KLacO signals, with different intensities (d); one signal dissociates in G1 (e), illustrating that clusters of KSHV plasmids can dissociate throughout the cell cycle. (B) Series of images illustrating the growth of clusters of miniKLacO and their segregation in SLK cells expressing LacI-tdTomato and LANA1 during three sequential mitoses. All signals increased in their intensities (given in the cartoons) close to twofold each S phase, as measured in CAPS (c, h, and l). The varying intensities are readily observed in Video 1 (part A), which shows consecutive uncompressed *z*-planes for several of the compressed images in this figure. Bars, 10 µm. See also Fig. S1 and Tables S1 and S2.

copy of *LacO* repeats and found them to double similarly over time (Fig. S1 E, a). The intensities of fluorescent beads stuck to the same surface as the cells in some of the samples with extrachromosomal signals were measured and found to vary less than 10% over 60 h, showing that the increase in intensities of miniKLacO corresponds to their duplication during S phase (Fig. S1 E, b).

Fluorescent signals in 11 parental cells were measured from early G1 and followed to early G1 of their daughter cells to assess the partitioning of clusters of plasmids. All of the intensities of the parents in G2 were inherited by the daughter cells (103 ± 3%), showing that the signals and the plasmids that yield them are conserved. The sum of these intensities was conserved even though the intensity of one signal in a daughter varied by 50-fold from that in its sibling (Fig. 5 B), demonstrating the frequent asymmetry of KSHV's partitioning. Clearly, clusters of KSHV plasmids can partition as units. These measurements, along with confocal microscopy (Fig. 5 C), confirmed another characteristic of the maintenance of miniKLacO plasmids we had found with intact KSHV: both the number and intensities of signals inherited by two daughter cells tended to be unequal (Figs. 3 B and 5 B and Table S2).

A computational model establishes that maintenance of KSHV plasmids depends on their clustering

Live-cell imaging of KLacO and miniKLacO plasmids as well as the analysis of unengineered KSHV genomes in PEL cells

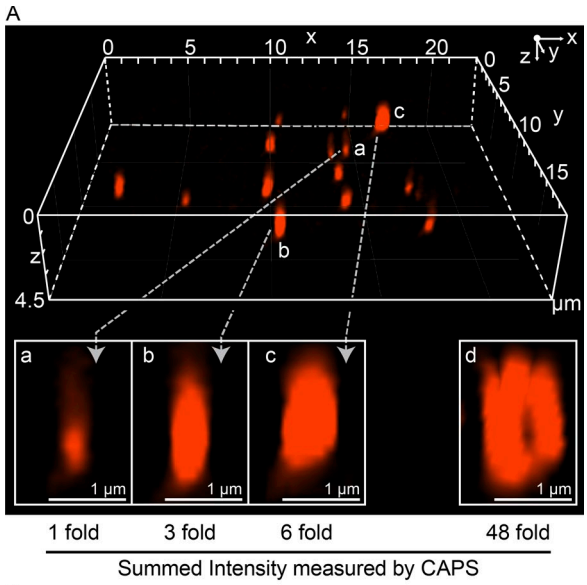

B

Ratio (qPCR amplicons/FISH signals per cell on average**)		
	EBV	KSHV
BC-1	0.97 (2.85/2.9)	1.3 (29.0/22)
BC-2	0.93 (3.85/4.2)	1.3 (39.0/30)

**p<0.0044 (KSHV vs.EBV; paired t-test)

Figure 4. **SIM of KSHV clusters and their detection in PEL cells.** (A) The distribution of size and intensities of miniKLacO clusters in SLK cells measured with SIM and CAPS confirms that, in general, they cannot be separated into smaller units. The structures of clusters in one cell (A) with up to sixfold differences in their intensities are homogeneous as resolved by SIM (a–c). A depth-encoded volume projection shows that the largest cluster (d), which has 48-fold higher intensity, is inhomogeneous. See also Video 2. (B) Numbers of KSHV and EBV genomes were measured by FISH and quantitative PCR in two PEL cell lines, BC-1 and BC-2, in the same cell populations and showed clustering of KSHV. Conventional FISH does not distinguish signals derived from one genome versus a cluster of genomes, whereas quantitative PCR measures the mean total number of viral genomes per cell in a population of cells. The number of viral genomes was quantified by detecting the copies of viral genes, *LANA1* for KSHV and *BALF5* for EBV, with linearized plasmid DNAs as standards and normalized to the copies of cellular *Rhodopsin*. These measurements (four experiments, two using BC-1 and two using BC-2) show that PEL cells have 30% of their KSHV genomes as clusters; as expected, EBV genomes do not cluster.

demonstrated that a fraction of these plasmids formed clusters and that these clusters could partition as units (Figs. 1, 2, 3, 4, and 5; and Tables S1 and S2). This mode of partitioning is without precedent, and so we sought an independent approach to confirm or refute this surprising discovery. We developed a computational model based solely on FISH and therefore independent of live-cell imaging data to analyze the replication of KSHV plasmids.

We monitored the distribution of KLacO and miniKLacO plasmids in proliferating cells with FISH after removing selection (Fig. 6 A). Two properties of the replication of KSHV plasmids were revealed by these measurements that would need to be substantiated in a successful computational model. First, cells lost KLacO signals as measured by FISH at a rate of 4% per generation and lost miniKLacO at a similar rate of 5% per generation (Fig. 6 A). Assuming that plasmids are lost from proliferating cells as a result of defects in synthesis, these rates of loss indicate that 90–92% of these plasmids are synthesized each S phase. Second, the distribution of signals in

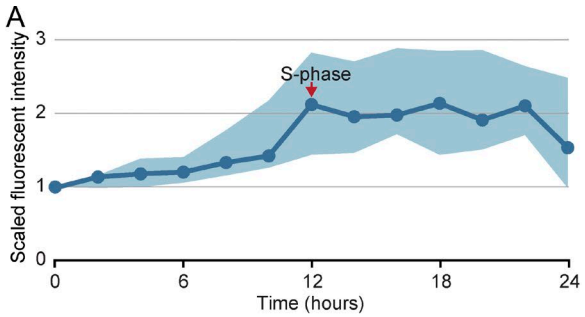

B A summary of the synthesis and partitioning of miniKLacO in SLK/WT LANA1 cells

Number of signals (Sum of intensities)				% of intensities in both daughters relative to parent
Parental cell		Daughter cells		
in G1	in G2	(A) in G1	(B) in G1	
7# (29k)	13 (62k)	7 (19k)	7 (43k)	100%
3 (53k)	6 (125k)	2 (17k)	5 (125k)	113%
7 (49k)	11 (88k)*	4 (34k)	7 (46k)	91%
1# (167k)	1 (358k)	1 (5k)	1 (309k)	88%
5 (47k)	5 (107k)	2 (42k)	3 (65k)	100%
2# (44k)	2 (86k)	1 (27k)	1 (70k)	113%
1 (65k)	2 (166k)	0 (0)	2 (159k)	96%
3 (65k)	3 (126k)	0 (0)	4 (139k)	111%
3 (67k)	6 (130k)*	4 (73k)	7 (80k)	118%
1 (22k)	1 (38k)	0 (0)	1 (41k)	107%
1 (41k)	1 (97k)	0 (0)	1 (97k)	100%
Sum				
34 (648k)	51 (1382k)	21 (217k)	39 (1173k)	

Summary: 34 signals in 11 cells in G1 were followed through a complete cell cycle to their daughter cells in G1; *The intensities of miniKLacO signals partition evenly into two daughter cells. # The number of miniKLacO signals partition evenly into two daughter cells.

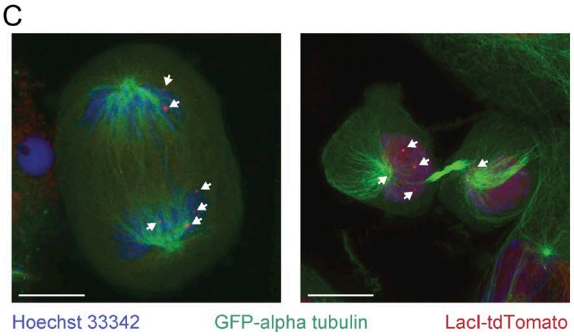

Figure 5. **Synthesis and unequal partitioning of KLacO and miniKLacO.** (A) The sum of intensities of miniKLacO signals in 24 cells followed for 60 h was determined with CAPS and scaled to 24 h for their progression from G1 through G2, with intensities at the beginning of G1 set to 1 and shown to double during S phase. The temporal scaling necessitated signals being binned; the SE for these bins is shaded in blue. (B) Shown are analyses of 11 cells with the distributions of miniKLacO signals and the sum of their intensities (a.u.) measured by CAPS in G1 through a complete cell cycle to their daughter cells in G1, illustrating their unequal partitioning (daughter cell B was arbitrarily assigned the higher-intensity signals). (C) SLK/wild-type LANA1 cells harboring miniKLacO and expressing the LacI-tdTomato fusion were transduced to express GFP-fused α-tubulin; 12 h after release from a double aphidicolin block, the signals of miniKLacO had different intensities and were distributed unevenly in separating two daughter cells in anaphase (left) or cytokinesis (right). Bars, 10 µm.

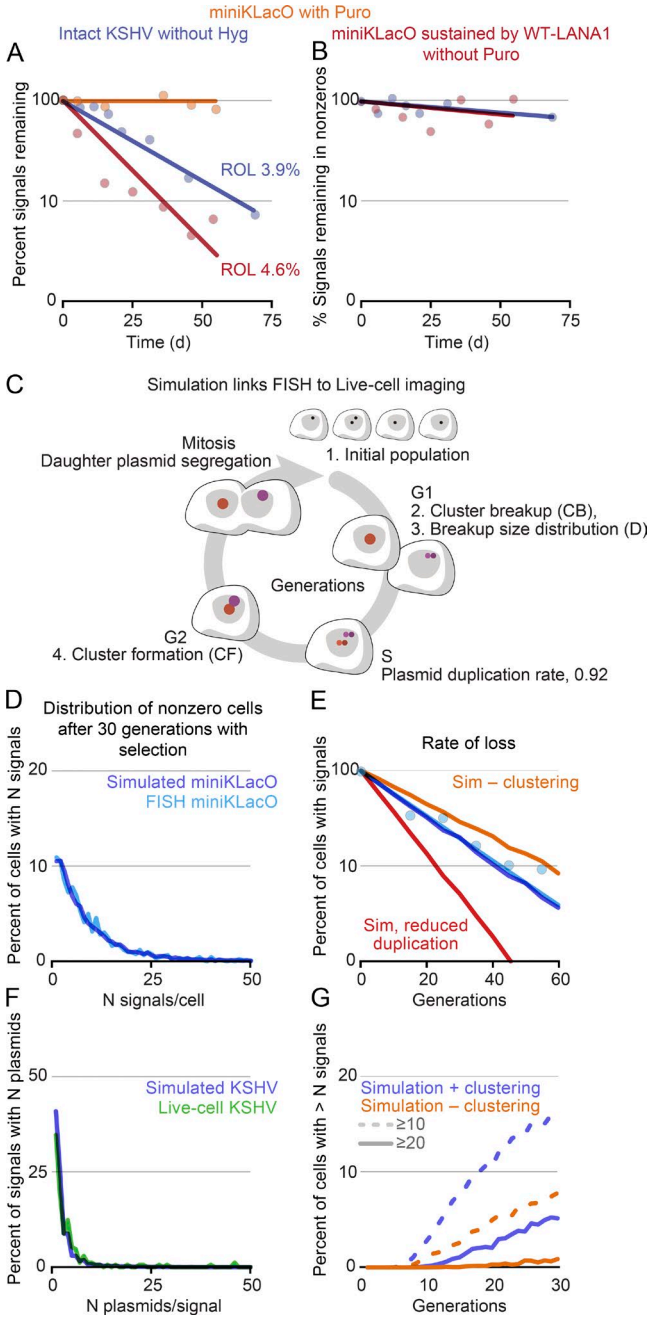

Figure 6. **Computer simulations based on FISH measurements predict findings with live-cell imaging.** (A and B) KLacO and miniKLacO signals were followed for 75 generations after removal of selection in two independent clones for each population with FISH. The percentage of signals remaining was measured at several time points. (A) KLacO signals and miniKLacO were lost from SLK or SLK/LANA1 cells at a rate of 3.9% and 4.6% (rate of loss [ROL]), respectively, per population doubling. (B) Although the majority of cells lost KLacO or miniKLacO during 75 doublings in the absence of selection, the percentage of signals remaining in a small fraction of cells were largely unchanged in their distribution. See also Fig. S1. (C) A summary of parameters used in the computer simulations and their predictions shown in the following panels, including the mean of the initial population, the probability of cluster breakup, and the size distribution of dissociated clusters. One parameter, the probability of cluster formation, was found to be optional. A final parameter, the probability of equal distribution between daughter plasmids, was varied only for the fusion protein shown in Fig. 8 D. (D) The distributions of miniKLacO signals after 30 generations without selection (light blue line) were predicted by computer simulations (dark blue line). Two clones of SLK/LacI-tdTomato cells expressing wild-type LANA1 and carrying miniKLacO were cultured without selection for 60 generations, and the distributions of miniKLacO signals were measured each 10 generations by FISH. (E) Varying the parameters in the simulations by removing clustering (orange line) or decreasing the efficiency of synthesis (red line) impaired the simulations. (F) Computer simulations based on FISH measurements predicted the number of miniKLacO plasmids per cluster observed in SLK/wild-type LANA1 cells using live-cell imaging. (G) Computer simulations predicted that clustering accelerates the accumulation of plasmids in a subset of newly infected/transfected cells. See also Materials and methods.

the cells that had not yet lost KLacO or miniKLacO signals remained largely unchanged over time, rather than drifting toward a distribution with fewer signals per cell (Fig. 6 B). This second property of KSHV's loss from cells in the absence of selection differs dramatically from that of EBV plasmids. EBV plasmids in the absence of selection are lost such that cells have fewer plasmids and the distribution of plasmids per cell tends to zero over time (Nanbo et al., 2007). These properties could not be recapitulated by simulating only the synthesis and partitioning of KSHV plasmids as independent elements. Rather, we found that the clustering of plasmids was required to develop a computational model that could recapitulate the replication of KSHV plasmids with these two properties.

The computational model was designed to reproduce both the rate at which cells without plasmids accumulated (a number dependent on the rate of loss of plasmids from cells but independent of the number of plasmids resident in the cells that have plasmids) and a stable distribution of plasmids among cells that retained them. The model was refined in a stepwise fashion to use only the minimum number of variables required, because matching data with small numbers of variables makes it less likely that the data have been misfitted (Dyson, 2004). We temporarily fixed partitioning to be random and added three variables to describe the formation and dissociation of clusters. These variables are the probability of cluster formation after S phase, the probability of cluster dissociation in the following G1 phase, and the resulting sizes of dissociated clusters (see Materials and methods).

In this simulation, first an initial population of unclustered plasmids is generated. Then, we simulate a plasmid duplication phase (S phase), a cluster formation phase (G2 phase), the allocation of clusters to daughter cells (M phase), and cluster dissociation (G1 phase; see Materials and methods; Fig. 6 C). Key to this simulation is that the partitioning behavior of individual plasmids can be varied, from preferentially moving to opposite daughter cells to preferentially moving to the same daughter cell within a cluster. Unlike faithful partitioning, clusters of plasmids can be maintained for multiple generations.

The variables were tested to cover all biological possibilities. The initial mean plasmids per cell were varied between six and 30, the probability of cluster formation in G2 ranged between 100% and 0%, the probability of breakup in G1 ranged between 0% and 100%, and the resulting cluster sizes were varied between breaking up into individual plasmids every time and splitting predominantly into two or more daughter clusters. To be able to test all possible combinations, we examined 200,000 variable combinations on the Open Science Grid and the University of Wisconsin–Madison Center for High Throughput Computing using HTCondor. The simulation with the optimal parameters with four variables yielded a distribution of nonzero plasmids per cell and rate of accumulation of cells with zero

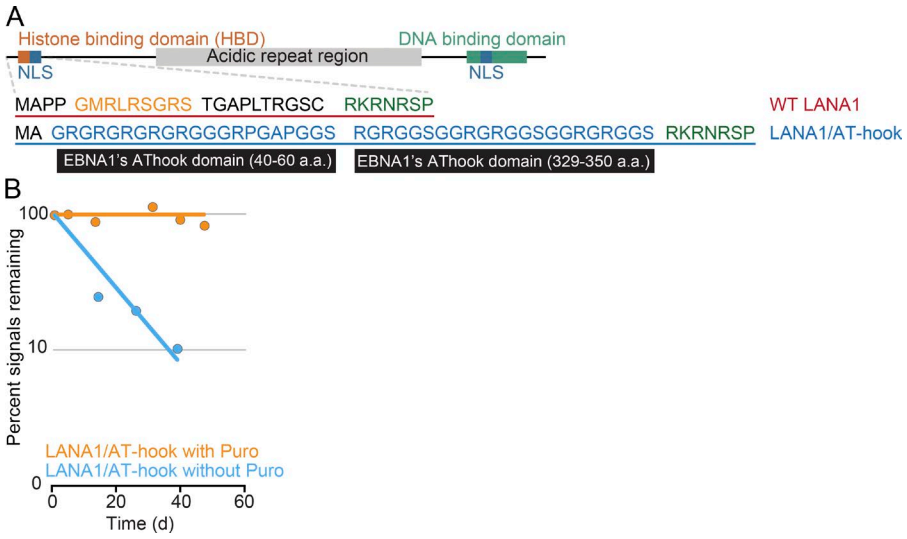

Figure 7. **Tethering KSHV to chromosomes is required for their synthesis.** (A) LANA1 and its derivatives are depicted with LANA1/dHBD in which the histone binding domain of LANA1 (HBD; aa 5–23) is deleted or replaced with the AT-hooks of EBNA1. (B) MiniKLacO signals in SLK cells expressing LANA1/AT-hook in two independent clones were followed without selection for 50 generations by FISH. MiniKLacO was lost from SLK/LANA1/AT-hook cells at a rate of 4.6% per generation.

plasmids that matched the FISH measurements of populations after 30 generations (Fig. 6, D and E, respectively). Varying the parameters by removing clustering or decreasing plasmid replication by 10% dramatically altered the results, which no longer represented those found with KSHV (Fig. 6 E). We determined that the rate of cluster formation in G2 did not affect our simulations as long as there were sufficient clusters to dissociate in G1. Therefore, we reduced our variables to three in all future simulations, with a fixed relationship (see Materials and methods) between the rate of cluster formation in G2 and breakup in G1.

The simulation, computed solely to match FISH measurements, recapitulated the distribution of cluster sizes derived from live-cell imaging (Fig. 6 F). It also independently supported the measurements of live-cell imaging by demonstrating that clustering of plasmids was necessary to produce the distribution of KSHV signals found in cells. This was done with only two variables describing clustering, which led to 38% probability of cluster formation in G2 and 31% probability of breakup in G1. These two probabilities yield an equilibrium in the number of clusters because some clusters break apart to give more than two smaller clusters.

In addition to reproducing the distributions of signals found in dynamic live-cell imaging from static FISH measurements, the simulation supported a strong evolutionary benefit for clustering: namely, that beginning with levels of one plasmid per cell, fewer generations are required for cells to reach higher copy numbers than for the quasi-faithful partitioning of EBV (Fig. 6 G). However, clustering increases the rate at which cells lose all copies of KSHV (Fig. 6 E). These findings underscore a contrast between EBV and KSHV: EBV's mechanism of partitioning maximizes the percentage of cells with plasmids, whereas KSHV's mechanism maximizes the number of plasmids per cell.

Identifying the mechanism of clustering of KSHV plasmids

EBV plasmids have not been found to cluster as do KSHV plasmids (Nanbo et al., 2007; Chiu et al., 2013). EBV uses the AT-hooks of EBNA1 to tether its plasmids directly to AT-rich chromosomal DNA, whereas LANA1 binds histones H2A and H2B within nucleosomes to tether KSHV plasmids indirectly to chromosomes (Marechal et al., 1999; Sears et al., 2004; Barbera et al., 2006; Chakravorty and Sugden, 2015). LANA1 also binds several cellular proteins, such as MeCP2, NuMA, Bub1, and CENP-F (Platt et al., 1999; Krithivas et al., 2002; Lim et al., 2003; Viejo-Borbolla et al., 2005; Ottinger et al., 2006; Matsumura et al., 2010; Xiao et al., 2010), which could contribute to tethering KSHV plasmids by these cellular proteins binding to chromosomal sites. The histone-binding domain of LANA1 is required for support of DNA synthesis of KSHV plasmids (Barbera et al., 2004). We tested whether it is also required for clustering by replacing it with the AT-hooks of EBNA1, introducing the vector encoding this LANA1/AT-hook fusion into SLK cells expressing LacI/tdTomato, and then introducing miniKLacO into the cells (Fig. 7 A).

Three complementary studies demonstrated that LANA1's binding of nucleosomes is essential for clustering KSHV plasmids. First, in cells expressing the fusion protein in the absence of selection, miniKLacO was lost at the same rate as in cells expressing wild-type LANA1 (Fig. 7 B). This rate indicated that the LANA1/AT-hook fusion supported the synthesis of KSHV plasmids at the same rate as does wild-type LANA1. Second, miniKLacO was visualized in live cells expressing the LANA1/AT-hook fusion over time (Fig. 8 A and Video 1 B). Its signals were quantified using CAPS; their intensities formed a near-Gaussian distribution consistent with their being one or two plasmids per signal and not forming clusters (Fig. 8 B). This distribution was wholly different from that formed by miniKLacO and KLacO in cells expressing wild-type LANA1, in which a fraction of signals had three- to 30-fold higher intensities than those in the cells expressing the LANA1/AT-hook fusion or in cells carrying latent visible EBV (Chiu et al., 2013) in 293 cells (Fig. 8 B). Third, the computational model could reproduce the population distributions measured by FISH in cells only after removing selection when it included plasmid clustering in the simulation for wild-type LANA1 (Fig. 6 E) but could do so only without clustering in the presence of LANA1/AT-hook (Fig. 8 C). This latter simulation was fitted only to the distribution of nonzero plasmids per cell, and it successfully predicted the rate of accumulation of cells with zero plasmids (Fig. 8 D).

LANA1 supports the clustering of KSHV plasmids; the LANA1/AT-hook fusion does not. Therefore, it is the ability of LANA1 to tether KSHV plasmids to histone pairs in nucleosomes that leads to the clustering of viral plasmids. We propose that LANA1 mediates clustering by binding site-specifically to TRs on one plasmid through its C-terminal DNA binding do-

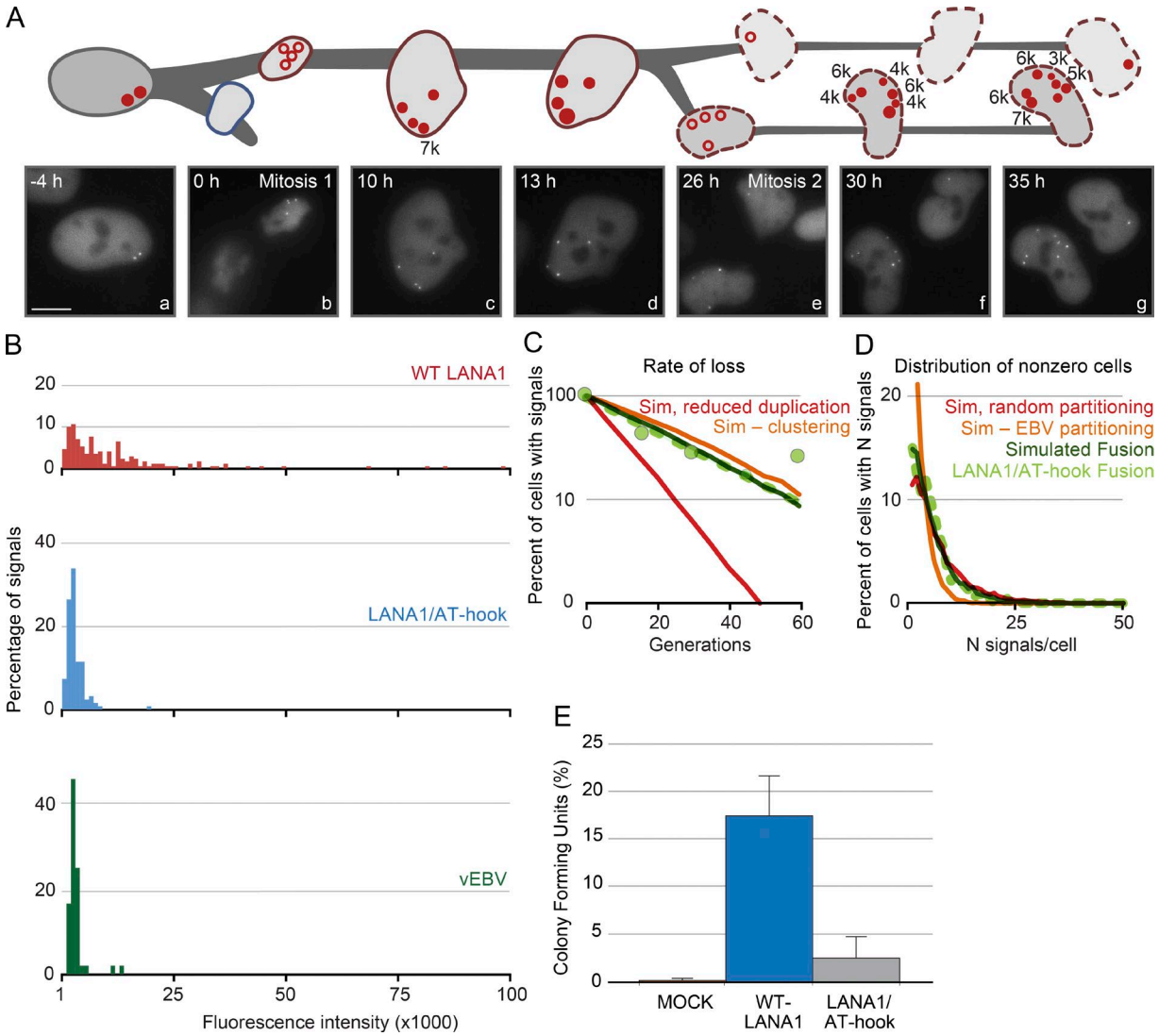

Figure 8. **Cluster formation of miniKLacO requires the N terminus of LANA and fosters plasmid establishment.** (A) MiniKLacO in SLK cells expressing LANA1/AT-hook was followed over 40 h using live-cell imaging. The cartoon and images with compressed signals are represented as described in the legend to Fig. 3. The varying intensities are readily observed in Video 1 (part B), which shows each consecutive *z*-plane for several of the compressed images in this figure. Bars, 10 µm. (B) Intensities of miniKLacO established in live SLK cells expressing wild-type LANA1 (red) or LANA1/AT-hook (blue), and those of visible EBV (green) in 293 cells were determined 3–4 h after mitosis (in G1 phase) with CAPS. They show that miniKLacO signals maintained by LANA1 are heterogeneous, with 100-fold differences in their intensities, whereas those maintained by LANA1/AT-hook or visible EBV are homogeneous, with two- to fourfold differences in intensities (wild-type LANA1, $n = 169$ signals; LANA1/AT-hook, $n = 121$ signals; vEBV, $n = 46$ signals). (C) Computer simulations predicted that the rate of loss of miniKLacO over time in cells expressing LANA1/AT-hook was insensitive to the absence of clustering but not to the rate of synthesis. (D) Two clones of SLK/LacI-tdTomato cells expressing LANA1/AT-hook and carrying miniKLacO were cultured without selection for 50 generations, and the distributions of miniKLacO signals were determined by FISH. The distributions of miniKLacO signals remaining in cells determined by FISH (light green line) were simulated (dotted blue line). A simulation using either the quasi-faithful partitioning of EBV (orange) or one using random partitioning (red) could not accurately reproduce the measured distributions. (E) WT LANA1 enhances colony formation relative to a derivative lacking its N terminus. SLK cells were transfected with a mock plasmid or plasmids expressing either wild-type LANA1 or LANA1/AT-hook along with miniKLacO and subsequently plated into selective media for 20 d to measure their colony-forming ability. The colony-forming unit was determined as a percentage of transfected cells resulting in puromycin-resistant colonies; error bars represent SDs obtained from three independent experiments. See also Fig. 7 and Table S3.

main and binding nucleosomes formed on the TRs of additional plasmids through its histone-binding domain. This bifunctional binding of TRs on multiple plasmids by LANA1 zippers plasmids together (Fig. 9).

A second insight from examining the distribution of KSHV plasmids supported by the LANA1/AT-hook fusion came from our simulations based on measurements with FISH. These simulations showed that partitioning mediated by the fusion protein was fitted best by plasmids being segregated equally to daughter cells 62% of the time (Fig. 8 D), which is more than for wild-type LANA1 and less than for wild-type EBNA1. When the simulations were modified explicitly to require the quasi-faithful partitioning observed for EBV (Nanbo et al., 2007), they did not fit the distributions measured for the LANA1/AT-hook fusion. These findings indicate that the AT-hooks of EBNA1 alone do not determine the quasi-faithful partitioning of EBV and that the histone-binding domain of LANA1 alone does not determine the random partitioning of KSHV. We propose that the distinct cis-acting elements of these two viral origins also contribute to the respective modes of viral partitioning.

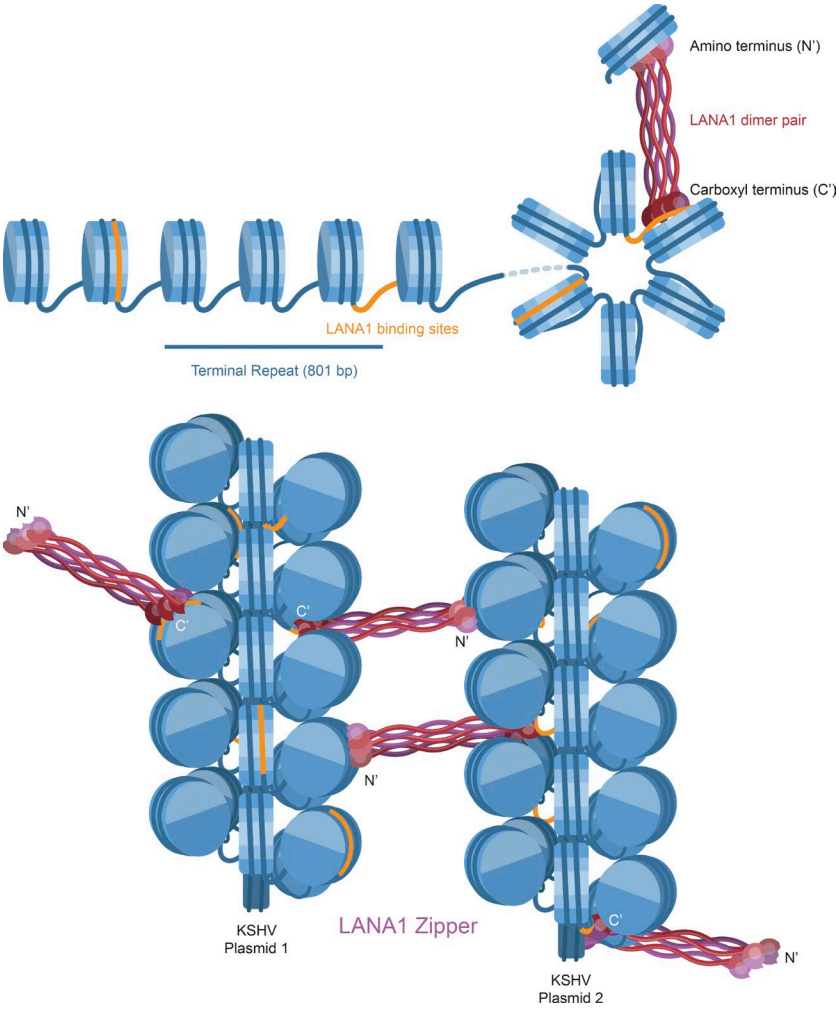

Figure 9. **Model of cluster formation of KSHV genomes.** Shown is a model depicting LANA1 tethering KSHV DNAs together through their TRs. The TRs, 801 bp in length, are blue lines wrapping nucleosomes with the orange segment representing the minimal replication element (MRE) with its three binding sites for the C termini of LANA1 dimers (Hellert et al., 2015). Three nucleosomes per TR accommodate the range of lengths of 192–277 bp per nucleosome used by Chodaparambil et al. (2007), who found that the N terminus of LANA1 on binding the faces of nucleosomes promotes their compaction into a 30-nm fiber (bottom). These compacted fibers have the C termini of LANA1 molecules bound to one KSHV genome's TRs, with their N termini bound to the nucleosomes on the TRs of other genomes.

How does clustering contribute to the replication of KSHV?

We compared and contrasted the replication of miniKLacO supported either by LANA1 or the LANA1/AT-hook fusion using live-cell imaging and our computational model (Figs. 3, 6, and 8). Live-cell imaging showed that replication supported by the LANA1/AT-hook fusion shares some properties with that supported by LANA1. For example, partitioning mediated by the fusion usually yielded daughter cells with unequal numbers of signals and often with different total intensities of signals (Table S3, A and B). The computational model further predicted that clustering drives the rapid accumulation of plasmids in a subset of cells (Fig. 6 G). We confirmed both this feature and the predictive robustness of the computational model by transfecting miniKLacO DNA into cells expressing either form of LANA1, selecting the cells in puromycin, and finding that wild-type LANA1 supported a 5- to 10-fold greater number of resistant colonies (Fig. 8 E). We know for both KSHV and EBV that establishment of colonies with transfected plasmids or infected cells is imperfect (Leight and Sugden, 2001; Grundhoff and Ganem, 2004). Experiments done with *oriP* plasmids have shown that this establishment depends on increases in the number of plasmids partitioned into daughter cells (Wang and Sugden, 2008). LANA1's clustering of plasmids thus facilitates KSHV's being established in newly infected cells.

Discussion

Both EBV and KSHV maintain themselves in lymphomas as plasmids. Both provide the tumor cells with selective advantages so that although only 85–90% of the viral plasmids are synthesized each cell cycle, they are found in effectively all of the tumor cells upon biopsy (Cesarman et al., 1995; Decker et al., 1996; Ballestas et al., 1999; Lindner and Sugden, 2007; Nanbo et al., 2007; Vereide and Sugden, 2011; Vereide et al., 2014). Both viruses have evolved mechanisms to partition themselves to daughter cells by using viral replication proteins to tether plasmid DNAs to host chromosomes. It is therefore startling to learn how different these mechanisms actually are.

The EBNA1 protein of EBV tethers the FR locus of *OriP* to AT-rich cellular DNA directly. This leads to roughly 90% of newly duplicated DNA being tethered individually to sister chromatids and quasi-faithful segregation (Nanbo et al., 2007). Faithful segregation leads to the maximum percentage of cells in a population containing plasmids. The strategy of maximizing the percentage of infected cells might seem to be optimal for a viral replicon.

KSHV, however, does not follow this strategy. The LANA1 protein of KSHV tethers the long contiguous track of 16 or more TRs (13,000 bp or more) to nucleosomes on other DNA molecules (Barbera et al., 2006), including additional KSHV plasmids. The resulting clusters of plasmids were de-

tected in PEL tumor cells grown in culture by both quantitative FISH (Fig. 1) and the combination of conventional FISH with quantitative PCR (Fig. 4 B). They could not in general be resolved into individual plasmids by high-resolution microscopy (Fig. 4 A) but were observed by live-cell imaging in SLK cells to grow in size, as measured by their increased intensities of bound Lac/tdTomato, and dissociate into smaller, less intense units over multiple cell cycles (Fig. 3, A and B). This tethering is to individual chromatids without any bias for sibling plasmids to associate with sister chromatids as has been found for EBV. Thus KSHV plasmids, over time, partition randomly (Fig. 5, B and C). It is not known whether other eukaryotic plasmids share KSHV's strategy for clustering its genomes; however, the yeast 2-µm circle does share properties with both KSHV and EBV and is a candidate for doing so (Liu et al., 2016).

Multiple studies of TR and LANA1 provide the background on which to picture clusters of these two elements. There are three close sites in each TR that can bind LANA1 dimers on the same face of the DNA (Hellert et al., 2015). The intervening ∼760 bp between each set of sites per TR is necessary for DNA synthesis (Shrestha and Sugden, 2014) and can accommodate three to four nucleosomes (Stedman et al., 2004). Clustering requires LANA1's N-terminal nucleosome-tethering domain (Fig. 7). Structural studies have shown that the N terminus of LANA1 bound to nucleosomes on DNA induces the formation of a 30-nm fiber (Chodaparambil et al., 2007). This structure would support the binding of up to 48 dimers of the C-terminal DNA-binding domain of LANA1 on one plasmid DNA to multiple additional nucleosome-bound plasmid DNAs (Fig. 9). We propose that the observed clusters of KSHV plasmids arise from LANA1 molecules on any one plasmid potentially binding nucleosomes on other KSHV plasmids.

Our computational simulations have shown that clusters are necessary to recapitulate the distributions of KSHV plasmids measured in fixed cells by FISH and in live cells by time-lapse fluorescence microscopy (Fig. 6, E–G). They also predicted that clustering of plasmids early in infection or transfection would drive rapid increases in the number of plasmids in a subset of cells, a property confirmed experimentally (Figs. 6 G and 8 E).

Multiple copies of the TR are selected for by KSHV; plasmids with only two or eight copies of the TR have been found to recombine often to yield derivatives with 16 or more copies of the TR when propagated in human cells (Shrestha and Sugden, 2014). This increase in the numbers of TRs in cis would favor clustering, an idea consistent with clustering itself being advantageous for the replication of KSHV.

It is imperative to understand the life cycles of human tumor viruses to develop specific antiviral and antitumor therapies. Such an understanding has led to the recent development of practical, effective vaccines for human papillomaviruses (Deleré et al., 2014). This understanding is particularly needed for KSHV and EBV, because only live-attenuated vaccines for herpesviruses have so far proven effective, and that class of vaccines cannot be used for tumor viruses (Wills et al., 2002; Kemble and Spaete, 2007; Chentoufi et al., 2012). These two human tumor viruses have evolved their own mechanisms to be maintained as plasmids in proliferating cells. These idiosyncratic mechanisms, although contrasting startlingly, have allowed both viruses to persist successfully as human pathogens. EBV has evolved to partition its genomes quasi-faithfully; KSHV often partitions its genomes as clusters, sacrificing equal partitioning for increased numbers of genomes in fewer cells.

Materials and methods

Cell lines and growth conditions

HeLa, SLK, and derivative cells were grown in DMEM containing 10% FBS. All PEL cells (JSC-1, BC1, and BC2) were obtained from the NIH AIDS Reagent Program and were grown in RPMI 1640 containing 10% FBS. All cells were maintained in a humidified 5% CO_2 incubator at 37°C. Cell lines are routinely screened for mycoplasma contamination using the primers described by van Kuppeveld et al. (1992). SLK cells were obtained from the NIH AIDS Reagent Program and are reported to be another cell line, Caki-1 (Stürzl et al., 2013). We have used the SLK name to maintain consistency with the literature. SLK cells were transduced and sorted for those with 30% mid-intensities of the LacI/tdTomato fusion (SLKmidTom). SLKmidTom cells were then transduced to express either wild-type LANA1 or LANA1/AT-hook followed by selection with 400 µg/ml hygromycin. Recombinant KSHV, KLacO, and miniKLacO were transfected into SLKmidTom to generate SLKmidTom(wild-type LANA1) or SLKmidTom(LANA1/AT-hook) cells, respectively, from single-cell clones that were resistant to 400 µg/ml hygromycin or 1 µg/ml puromycin, respectively.

Plasmids

pMHGP (Zhou et al., 2002), provided by S.-J. Gao (University of Southern California, Los Angeles, CA), was modified to replace eGFP with ∼250 copies of the lactose operator sequence (*lacO*), resistance to kanamycin under a prokaryotic promoter, and ∼1.5 kbp of KSHV sequence located adjacent to the BAC insert region of BAC36 (encoding *ORF19*), generating p3615. The DNA fragment of p3615 linearized with restriction enzymes NotI and DraIII was then transformed into *Escherichia coli* DH10B (pKD46, KSHV BAC36) to generate KLacO via red-mediated recombination (Norby et al., 2012). Kanamycin-resistant colonies were screened by PCR for the insertion of antibiotic-resistant genes and the junction with BAC36, and further by restriction digestion to confirm the integrity of the Bacmid. The length/copy number of *lacO* was determined by Southern blotting after restriction digestion. MiniKLacO (p4156) is derived from a plasmid encoding 16 copies of KSHV TRs and puromycin resistance (Shrestha and Sugden, 2014) by introducing a DNA fragment of 250 copies of *lacO* sequence from pLON (Nanbo et al., 2007). A DNA fragment encoding wild-type LANA1 was inserted into a bicistronic internal ribosomal entry site (IRES)-*hygromycin*^{R} retroviral vector, p3920 (Shrestha and Sugden, 2014). The DNA fragment that encodes the third through 23rd residues of LANA1 in p3920 was deleted with the Gibson assembly method (New England Biolabs, Inc.) to generate p4187 (pLANA1/dHBD). A gene block encoding the AT-hook domains of EBNA1 (GRGRGRGRGRGGGRPGAPGGSRGR GGSGGRGRGGSGGRGRGGS) was synthesized (Integrated DNA Technologies) and used to substitute the third through 23rd residues of LANA1 in the bicistronic IRES-*Hygromycin*^{R} retroviral vector with the Gibson assembly method to generate p4189 (pLANA1/AT-hook). A DNA fragment encoding the GFP-fused α-tubulin was digested from pEGFP-TUB (Takara Bio, Inc.) with NheI and BamHI and inserted into the HpaI–BamHI site of a retroviral vector, p3048. A tetrameric LacI was fused translationally with the tdTomato fluorescent protein into a retroviral vector, p4001 (Chiu et al., 2013). The EBV replication origin, DS, was removed from pLON (Nanbo et al., 2007) with SnaBI and SpeI and substituted by a SpeI–DraI DNA fragment encoding 16 copies of KSHV TRs to generate pminiKLacOplusFR (p4066).

Time-lapse experiments

Time-lapse experiments were performed with an image system using an Axiovert 200M microscope (ZEISS) equipped with a Colibri LED illumination system and a 37°C incubation system as described

(Norby et al., 2012). Cells were maintained in DMEM containing 10% FBS. 90 *z*-planes were sampled at intervals of 0.35 µm, every 60 min over 60 h, using Axiovision 4.8.2. 150-ms exposure times for tdTomato red signals were chosen to allow detection of signals with minimal exposures. All images were collected with a Plan-Apo 63× (NA 1.40) oil objective (ZEISS; for experiments with KLacO) or an Alpha Plan-Apo 100× (NA 1.46) oil objective (ZEISS; for experiments with miniKLacO) and a Cascade II:1024 EMCCD camera (Photometrics) with a 16-bit dynamic range. No images were saturated as judged by their most intense pixels being less than half of ∼65,000 available gray levels. All images acquired in live cells were analyzed with CAPS, which uses photometry with subtraction of a background derived from an annulus of the pixels over multiple *z*-planes surrounding a given LacI-fluorescent signal of KSHV derivatives (Chiu et al., 2013).

Superresolution experiments

Superresolution microscopy experiments were performed with a Nikon N-SIM microscope with a Apochromat TIRF 100× oil objective (NA 1.49). During imaging, cells were maintained at room temperature in phenol red–free DMEM containing 10% FBS and Hepes. All images of tdTomato were collected with an iXon 897 EMCCD camera (Andor Technology) using a 561-nm laser with the microscope in 3D SIM mode. N-SIM reconstruction, linear intensity adjustment, volume rendering (MaxIP), and movie production were performed in NIS-Elements Ar version 4.50.00 (Nikon). Final video with annotations presented as Video 2 was produced in kdenlive.

Production of retroviruses and transduction

Retroviral vectors were generated in 293T cells as previously described (Chiu et al., 2013), with modifications. Briefly, retrovirus was generated by cotransfecting 293T in a 70% confluent 10-cm dish with 3 µg of a plasmid encoding Gag-Pol, 1 µg of a plasmid encoding the vesicular stomatitis virus G protein, 1 µg of a plasmid encoding a derivative of NF-κB, and 10 µg of a plasmid carrying the retroviral backbone containing genes encoding a LacI-tdTomato fusion or an EGFP-α-tubulin fusion using Lipofectamine 2000 (Thermo Fisher Scientific). The viruses were collected from the culture medium 24 and 48 h after transfection, followed by sedimentation in a 50Ti rotor at 25,000 rpm for 2 h. SLK cells were then incubated with concentrated virus stocks at 4°C for 1 h followed by 37°C for 48 h for retrovirus infection.

Short-term replication assay

Short-term replication assays were performed as described (Shrestha and Sugden, 2014). In brief, 293 cells were cotransfected with 2 µg peGFP-C1 (Takara Bio Inc.; as a control for transfection efficiency), 15 µg miniKLacO plasmids and 8 µg of p3920, p4187, or p4189 using Lipofectamine 2000 according to the manufacturer's recommended protocol. The transfection efficiency was determined as the percentage of GFP-positive cells 2 d after transfection. 100 µg DNA was isolated from cells 4 d post-transfection with the Hirt extraction method (Hirt, 1967) and digested with 80 U HindIII overnight to linearize the plasmids being assayed. 70% of the HindIII-digested DNA was digested further with 100 U DpnI overnight to distinguish the newly synthesized plasmids from the unsynthesized and bacterially methylated DNAs, followed by Southern blotting.

Southern blotting

Southern blotting was performed as described (Wang and Sugden, 2008). Depurinated DNA was denatured and transferred to GeneScreen Plus hybridization membranes (NEN Life Sciences) by capillary action with 10× SSC buffer overnight followed by UV cross-linking. ^{32}P-radiolabeled DNA fragments were prepared using a Rediprime II Random Prime Labeling System (GE Healthcare) as described by the manufacturer and hybridized to the DNA on the membrane in ULTRAhyb hybridization buffer (Ambion) at 42°C overnight. After two washes with 2× SSC buffer with 0.1% SDS at 60°C for 15 min and twice with a buffer containing 0.1× SSC and 0.1% SDS at 55°C for 15 min, the hybridized membrane was exposed to a Storage Phosphor Screen, and the signals were captured using a Storm PhosphorImager (Molecular Dynamics).

Gardella Gel

Gardella gels were performed as described (Gardella et al., 1984; Shrestha and Sugden, 2014) to ensure that KSHV genome derivatives were maintained extrachromosomally in cells. Each Gardella gel, which was cast as a horizontal 20 × 28-cm (width by length) gel, consisted of (a) a resolution gel made of 0.75% agarose in 1× Tris-borate-EDTA (TBE) buffer, pH 8.2, and (b) a lysis gel made of 0.8% agarose, 2% SDS, and 1 mg/ml proteinase K in 1× TBE buffer. The lysis gel occupied the top 5 cm of the horizontal gel and included a comb consisting of 10 × 1 × 6-mm (width by depth by height) wells for loading samples. Cells resuspended in 50 µl resuspension buffer (7% Ficoll, 100 µg/ml RNase A, and 0.01% bromophenol blue in PBS) were loaded into the wells and electrophoresed initially at 0.8 V/cm for 3–4 h and then at 4.5 V/cm for ∼16 h at 4°C. Upon completion, the gel was stained with 0.5 µg/ml ethidium bromide in 1× TBE for 20 min, visualized with UV, and analyzed by Southern blotting.

Colony-forming assay

SLKmidTom cells were transduced to express both wild-type LANA1 or AT-hook-LANA1 and eGFP from a bicistronic transcript with an IRES and sorted for those with similar expression levels of eGFP to reflect the levels of expression of LANA1 derivatives by flow cytometry. The sorted cells expressing either wild-type LANA1 or AT-hook LANA1 in 10-cm plates when 80% confluent were cotransfected with 20 µg miniKLacO, and the same number of parental SLKmidTom cells were transfected with pMaxi-GFP, a GFP expression plasmid, using Lipofectamine. 2 d after transfection, the GFP-positive cells were counted to determine the transfection efficiency. The successfully transfected cells were plated at 100, 300, 10^3, 3×10^3, and 10^4 cells per 15-cm plate and selected with 1 µg/ml puromycin. The resistant colonies were counted to determine the colony-forming efficiency after selection for 2 wks. The number of colonies from each set of transfected cells was normalized to the transfection efficiency.

Fluorescent in situ hybridization

FISH analysis was performed as described (Nanbo et al., 2007). In brief, cells were treated with 0.075 M KCl for 20 min at 37°C, fixed in methanol:acetic acid at a 3:1 ratio for 30 min at room temperature, and spread on cold slides. Slides were dried and prehybridized in a buffer with 4× SSC and 0.5% (vol/vol) Nonidet P-40 (Sigma-Aldrich) for 30 min at 37°C, dehydrated in a cold ethanol series (70%, 80%, and 90%) for 2 min each, air-dried at 50°C, denatured in a buffer with 70% formamide and 2× SSC, pH 5.3, for 2 min at 72°C followed by dehydration with a cold ethanol series, and air-dried. The KSHV cosmid Z8 (Russo et al., 1996) or miniKLacO was labeled with digoxigenin-11-2′-deoxy-uridine-5′-triphosphate (Roche), and EBV p138.2 was labeled with biotin-16-dUTP (Roche) by nick translation as hybridization probes for detection of KLacO or miniKLacO and EBV in cells, respectively. 20 µg of the labeled probe was precipitated along with 6 µg salmon sperm DNA and 4 µg human Cot-1 DNA (Invitrogen) and resuspended in CEP hybridization buffer (55% formamide, 1× SSC,

pH 7.0, and 10% dextran sulfate) followed by denaturation at 70°C for 10 min. 5 ng of the probe was then hybridized with each sample at 37°C overnight in a moist chamber. The slides were washed twice in 2× SSC containing 50% formamide for 30 min at 50°C and twice in 2× SSC for 30 min at 50°C. The hybridized probe was detected by incubation with 10 µl of a detection solution containing a mouse monoclonal anti-digoxin–FITC conjugate (Sigma-Aldrich) and a streptavidin-Cy3 conjugate (Sigma-Aldrich) for 20 min at 37°C. The slides were washed twice in 4× SSC containing 0.05% Triton X-100 for 5 min at room temperature and mounted in Vectashield antifading media with DAPI (Vector Laboratories) for staining chromosomes.

FISH slides were imaged on an Axiovert 200M microscope (described in Time-lapse experiments) at room temperature. For intensity measurements, images acquired were analyzed with CAPS (Chiu et al., 2013). The brightness of the KSHV panel in Fig. 1 A was reduced using Photoshop CC 2015 so that the mean of all pixels was approximately equal to the mean of all pixels for the EBV panel. This linear adjustment was applied to the entire image and is used for display purposes only.

Synchronization and imaging of mitotic cells

Cells were synchronized at S phase with 15 µM aphidicolin for 16 h, washed five times in complete medium, and grown in the absence of aphidicolin for 8 h. They were treated again with 15 µM aphidicolin for 16 h and washed five times with complete medium to remove aphidicolin. Cells released from double-aphidicolin block were fixed with 4% PFA every hour after releasing the cells from the second block for 8 h and stained for chromosomes with Hoechst dye. Cells were mounted in Vectashield antifading media without DAPI (Vector Laboratories). GFP, tdTomato, and Hoechst in the mitotic cells were imaged at room temperature with an Olympus FluoView FV1000 confocal microscope with a 100× (NA 1.45) oil objective using Fluoview (Olympus).

Computer model and HTCondor

The dynamics of the synthesis, partitioning, and clustering of KSHV plasmids was incorporated into a software model written to be compatible with Python 2.7. The software model was used for initial simulations performed on HTCondor, a distributed-computing system that allows examination of a diverse parameter space. After the initial parameter space was refined through the initial simulations, additional simulations were performed locally. Source code is included as a zip file in the online supplemental material. Source code for local and HTCondor implementations are available at https://bitbucket.org/asugden/plasmid-replicator-crp. Additional information on the parameters used for initial simulations and a flowchart detailing the structure of the software model is provided in that Bitbucket repository. Pseudocode, which provides a simplified depiction of the software model, is provided in the online supplemental material zip file.

Definition and variations of parameters used in computer model and HTCondor

We used the findings described by Nanbo et al. (2007) to build the framework for the model presented in this paper. We modeled the maintenance of plasmids as the combination of replication, in which a plasmid may be duplicated in S phase, and partitioning, when the daughter plasmids are distributed to daughter cells. Because we found that KSHV plasmids in the presence of LANA1 can form clusters, we incorporated the ability of individual plasmids to come together to form clusters and for clusters to break up resulting in smaller clusters or individual plasmids. The program we created to use this model, ReplicatorII, is written for Python 2.7. Source code and extensive documentation can be found at the Bitbucket repository mentioned in the previous section.

An important feature of the implementation of our model is that many parameters can be varied for a simulation. For example, the probability that a plasmid replicates in a given S phase can be modified. Cluster formation and breakup were simulated using a stochastic algorithm termed the "Chinese restaurant process."

Each simulation begins with burn-in generations that use the provided parameters to generate an initial population of cells with a distribution of plasmids determined by the input parameters. This is followed by the simulation, which we ran for 30 simulated cell cycles. This was then repeated for a total of 10 times for each input parameter combination, and the results were averaged. The program is provided with a dataset consisting of plasmid distributions of cells measured with FISH. This provides the comparison to determine whether the simulation approximated the experimentally observed distribution. The program then quantifies the difference between the simulation and the experimental results.

Initial simulations were run using HTCondor. Each set of parameters was run 10 times for 30 generations after 50 burn-in generations, and the results were averaged. We "flocked" on the UW-campus and "glided" into the OSG. Definitions of these parameters and values, which were used in the HTCondor simulations of wtLANA1, are provided at the Bitbucket repository. The output was then analyzed to determine the parameter space that produced plasmid distributions consistent with the observed FISH data. Then more simulations were run locally to confirm the results from the HTCondor simulations and generate the figures in the article.

The cell replication equation to determine whether a particular cell (with n plasmids) replicates is as follows: $P(\text{cell replicates}|a,b,c) = c - a \times x^2 - b \times x$, where x = n_plasmids_per_cell, a = signal-selective-disadvantage-on-cell-replication-squared, b = signal-selective-disadvantage-on-cell-replication, and c = mean-cell-replication-prob.

Statistics

The Kolmogorov–Smirnov test and paired t test were performed using Python 2.7, Pandas 0.19.1, and SciPy 0.17.0.

Online supplemental material

Fig. S1 shows control data demonstrating that the replication of KLacO is licensed, its presence does not affect cell viability, and the fluorescent intensity of integrated signals approximately doubles during S phase. Table S1 contains data on the distribution of KLacO signals across mitosis. Table S2 contains similarly arranged data for miniKLacO. Table S3 shows the distribution of miniKLacO signals and summed intensities across mitosis in cells expressing the fusion protein, LANA1/AT-hook. Video 1 details how CAPS was used to analyze z-stacks collected from living cells. Specifically, data underlying Figs. 3 and 8 are shown. Video 2 presents rotations about a volumetric rendering of miniKLacO genomes in SLK cells. Static images of this data are presented in Fig. 4. A zip file contains the following seven files relating to the simulations. pseudocode.txt contains a simplified depiction of the software model. README.MD contains information on running simulations locally. ReplicatorII.py contains the main code (in Python) for the simulations. Replicator-crp-pars.txt contains parameter values used for a simulation. Four files for running simulations on HTCondor are included. pars_generator.py is a python script for generating parameter files used by each worker node. start.sh is a bash script for executing the simulations on each worker node. minimal-data-copy.sh is a script to run on the submit node after job completion to filter out logging information. condor-output-combiner.py merges the results of many HTCondor jobs into a single .csv file for simpler file handling. Checksums.sha256 contains checksums for these files.

Acknowledgments

We thank Drs. Edwin R. Chapman and Ewa Bomba-Warczak for support with the Olympus FluoView FV1000 confocal microscope, Dr. Prabha Shrestha for p4066, and Dr. Elle Grevstad of University of Wisconsin–Madison Biochemistry Optical Core for her expert help with N-SIM. We thank Drs. Paul Ahlquist, Norman Drinkwater, Nathan Sherer, and Eric Johannsen and our laboratory colleagues for their experimental insights and suggestions.

This work was funded by grants from the National Cancer Institute (P01 CA022443, R01 CA133027, and R01 CA070723), the Ministry of Science and Technology, Taiwan (MOST-105-2320-B-182-033), the National Health Research Institute (NHRI-EX106-10623BI), Chang Gung Memorial Hospital, Linkou (BMR PF14), and the Morgridge Institute for Research. B. Sugden is an American Cancer Society Research Professor. This simulation was performed using the computer resources and assistance of the University of Wisconsin–Madison Center for High Throughput Computing (CHTC) in the Department of Computer Sciences. The CHTC is supported by the University of Wisconsin–Madison, the National Science Foundation, and the U.S. Department of Energy's Office of Science. The cell sorting facility is supported by a grant from the University of Wisconsin Carbone Cancer Center (P30 CA014520).

The authors declare no competing financial interests.

Author contributions: Y.-F. Chiu, K. Fox, M. Hayes, and B. Sugden designed the study and performed biochemistry and live-cell imaging analyses. A.U. Sugden contributed the program, CAPS, for computational analysis. A.U. Sugden and M. Hayes contributed the computational simulation and HTCondor programing. All authors worked together to write the manuscript.

Submitted: 2 February 2017
Revised: 23 May 2017
Accepted: 31 May 2017

References

Bais, C., B. Santomasso, O. Coso, L. Arvanitakis, E.G. Raaka, J.S. Gutkind, A.S. Asch, E. Cesarman, M.C. Gershengorn, and E.A. Mesri. 1998. G-protein-coupled receptor of Kaposi's sarcoma-associated herpesvirus is a viral oncogene and angiogenesis activator. *Nature.* 391:86–89. http://dx.doi.org/10.1038/34193

Ballestas, M.E., and K.M. Kaye. 2001. Kaposi's sarcoma-associated herpesvirus latency-associated nuclear antigen 1 mediates episome persistence through cis-acting terminal repeat (TR) sequence and specifically binds TR DNA. *J. Virol.* 75:3250–3258. http://dx.doi.org/10.1128/JVI.75.7.3250-3258.2001

Ballestas, M.E., P.A. Chatis, and K.M. Kaye. 1999. Efficient persistence of extrachromosomal KSHV DNA mediated by latency-associated nuclear antigen. *Science.* 284:641–644. http://dx.doi.org/10.1126/science.284.5414.641

Barbera, A.J., M.E. Ballestas, and K.M. Kaye. 2004. The Kaposi's sarcoma-associated herpesvirus latency-associated nuclear antigen 1 N terminus is essential for chromosome association, DNA replication, and episome persistence. *J. Virol.* 78:294–301. http://dx.doi.org/10.1128/JVI.78.1.294-301.2004

Barbera, A.J., J.V. Chodaparambil, B. Kelley-Clarke, V. Joukov, J.C. Walter, K. Luger, and K.M. Kaye. 2006. The nucleosomal surface as a docking station for Kaposi's sarcoma herpesvirus LANA. *Science.* 311:856–861. http://dx.doi.org/10.1126/science.1120541

Carbone, A., E. Cesarman, A. Gloghini, and H.G. Drexler. 2010. Understanding pathogenetic aspects and clinical presentation of primary effusion lymphoma through its derived cell lines. *AIDS.* 24:479–490. http://dx.doi.org/10.1097/QAD.0b013e3283365395

Cesarman, E., P.S. Moore, P.H. Rao, G. Inghirami, D.M. Knowles, and Y. Chang. 1995. In vitro establishment and characterization of two acquired immunodeficiency syndrome-related lymphoma cell lines (BC-1 and BC-2) containing Kaposi's sarcoma-associated herpesvirus-like (KSHV) DNA sequences. *Blood.* 86:2708–2714.

Chakravorty, A., and B. Sugden. 2015. The AT-hook DNA binding ability of the Epstein Barr virus EBNA1 protein is necessary for the maintenance of viral genomes in latently infected cells. *Virology.* 484:251–258. http://dx.doi.org/10.1016/j.virol.2015.05.018

Chaudhuri, B., H. Xu, I. Todorov, A. Dutta, and J.L. Yates. 2001. Human DNA replication initiation factors, ORC and MCM, associate with oriP of Epstein-Barr virus. *Proc. Natl. Acad. Sci. USA.* 98:10085–10089. http://dx.doi.org/10.1073/pnas.181347998

Chentoufi, A.A., E. Kritzer, D.M. Yu, A.B. Nesburn, and L. Benmohamed. 2012. Towards a rational design of an asymptomatic clinical herpes vaccine: The old, the new, and the unknown. *Clin. Dev. Immunol.* 2012:187585.

Chiu, Y.F., A.U. Sugden, and B. Sugden. 2013. Epstein-Barr viral productive amplification reprograms nuclear architecture, DNA replication, and histone deposition. *Cell Host Microbe.* 14:607–618. http://dx.doi.org/10.1016/j.chom.2013.11.009

Chodaparambil, J.V., A.J. Barbera, X. Lu, K.M. Kaye, J.C. Hansen, and K. Luger. 2007. A charged and contoured surface on the nucleosome regulates chromatin compaction. *Nat. Struct. Mol. Biol.* 14:1105–1107. http://dx.doi.org/10.1038/nsmb1334

Cotter, M.A. II, and E.S. Robertson. 1999. The latency-associated nuclear antigen tethers the Kaposi's sarcoma-associated herpesvirus genome to host chromosomes in body cavity-based lymphoma cells. *Virology.* 264:254–264. http://dx.doi.org/10.1006/viro.1999.9999

Decker, L.L., P. Shankar, G. Khan, R.B. Freeman, B.J. Dezube, J. Lieberman, and D.A. Thorley-Lawson. 1996. The Kaposi sarcoma-associated herpesvirus (KSHV) is present as an intact latent genome in KS tissue but replicates in the peripheral blood mononuclear cells of KS patients. *J. Exp. Med.* 184:283–288. http://dx.doi.org/10.1084/jem.184.1.283

Deleré, Y., O. Wichmann, S.J. Klug, M. van der Sande, M. Terhardt, F. Zepp, and T. Harder. 2014. The efficacy and duration of vaccine protection against human papillomavirus: A systematic review and meta-analysis. *Dtsch. Arztebl. Int.* 111:584–591.

Dhar, S.K., K. Yoshida, Y. Machida, P. Khaira, B. Chaudhuri, J.A. Wohlschlegel, M. Leffak, J. Yates, and A. Dutta. 2001. Replication from oriP of Epstein-Barr virus requires human ORC and is inhibited by geminin. *Cell.* 106:287–296. http://dx.doi.org/10.1016/S0092-8674(01)00458-5

Dyson, F. 2004. A meeting with Enrico Fermi. *Nature.* 427:297. http://dx.doi.org/10.1038/427297a

Gao, S.J., C. Boshoff, S. Jayachandra, R.A. Weiss, Y. Chang, and P.S. Moore. 1997. KSHV ORF K9 (vIRF) is an oncogene which inhibits the interferon signaling pathway. *Oncogene.* 15:1979–1985. http://dx.doi.org/10.1038/sj.onc.1201571

Gardella, T., P. Medveczky, T. Sairenji, and C. Mulder. 1984. Detection of circular and linear herpesvirus DNA molecules in mammalian cells by gel electrophoresis. *J. Virol.* 50:248–254.

Giffin, L., and B. Damania. 2014. KSHV: pathways to tumorigenesis and persistent infection. *Adv. Virus Res.* 88:111–159. http://dx.doi.org/10.1016/B978-0-12-800098-4.00002-7

Grundhoff, A., and D. Ganem. 2004. Inefficient establishment of KSHV latency suggests an additional role for continued lytic replication in Kaposi sarcoma pathogenesis. *J. Clin. Invest.* 113:124–136. http://dx.doi.org/10.1172/JCI200417803

Guasparri, I., S.A. Keller, and E. Cesarman. 2004. KSHV vFLIP is essential for the survival of infected lymphoma cells. *J. Exp. Med.* 199:993–1003. http://dx.doi.org/10.1084/jem.20031467

Hammerschmidt, W., and B. Sugden. 2013. Replication of Epstein-Barr viral DNA. *Cold Spring Harb. Perspect. Biol.* 5:a013029. http://dx.doi.org/10.1101/cshperspect.a013029

Hellert, J., M. Weidner-Glunde, J. Krausze, H. Lünsdorf, C. Ritter, T.F. Schulz, and T. Lührs. 2015. The 3D structure of Kaposi sarcoma herpesvirus LANA C-terminal domain bound to DNA. *Proc. Natl. Acad. Sci. USA.* 112:6694–6699. http://dx.doi.org/10.1073/pnas.1421804112

Hirt, B. 1967. Selective extraction of polyoma DNA from infected mouse cell cultures. *J. Mol. Biol.* 26:365–369. http://dx.doi.org/10.1016/0022-2836(67)90307-5

Hodin, T.L., T. Najrana, and J.L. Yates. 2013. Efficient replication of Epstein-Barr virus-derived plasmids requires tethering by EBNA1 to host chromosomes. *J. Virol.* 87:13020–13028. http://dx.doi.org/10.1128/JVI.01606-13

Hu, J., A.C. Garber, and R. Renne. 2002. The latency-associated nuclear antigen of Kaposi's sarcoma-associated herpesvirus supports latent DNA replication in dividing cells. *J. Virol.* 76:11677–11687. http://dx.doi.org/10.1128/JVI.76.22.11677-11687.2002

Kemble, G., and R. Spaete. 2007. Herpes simplex vaccines. *In* Human Herpesviruses: Biology, Therapy, and Immunoprophylaxis. A. Arvin, G. Campadelli-Fiume, E. Mocarski, P.S. Moore, B. Roizman, R. Whitley,

and K. Yamanishi, editors. Cambridge University Press, Cambridge, UK. http://dx.doi.org/10.1017/CBO9780511545313.070

Krithivas, A., M. Fujimuro, M. Weidner, D.B. Young, and S.D. Hayward. 2002. Protein interactions targeting the latency-associated nuclear antigen of Kaposi's sarcoma-associated herpesvirus to cell chromosomes. *J. Virol.* 76:11596–11604. http://dx.doi.org/10.1128/JVI.76.22.11596-11604.2002

Lee, H., R. Veazey, K. Williams, M. Li, J. Guo, F. Neipel, B. Fleckenstein, A. Lackner, R.C. Desrosiers, and J.U. Jung. 1998. Deregulation of cell growth by the K1 gene of Kaposi's sarcoma-associated herpesvirus. *Nat. Med.* 4:435–440. http://dx.doi.org/10.1038/nm0498-435

Leight, E.R., and B. Sugden. 2001. Establishment of an oriP replicon is dependent upon an infrequent, epigenetic event. *Mol. Cell. Biol.* 21:4149–4161. http://dx.doi.org/10.1128/MCB.21.13.4149-4161.2001

Lieberman, P.M. 2013. Keeping it quiet: Chromatin control of gammaherpesvirus latency. *Nat. Rev. Microbiol.* 11:863–875. http://dx.doi.org/10.1038/nrmicro3135

Lim, C., D. Lee, T. Seo, C. Choi, and J. Choe. 2003. Latency-associated nuclear antigen of Kaposi's sarcoma-associated herpesvirus functionally interacts with heterochromatin protein 1. *J. Biol. Chem.* 278:7397–7405. http://dx.doi.org/10.1074/jbc.M211912200

Lindner, S.E., and B. Sugden. 2007. The plasmid replicon of Epstein-Barr virus: Mechanistic insights into efficient, licensed, extrachromosomal replication in human cells. *Plasmid.* 58:1–12. http://dx.doi.org/10.1016/j.plasmid.2007.01.003

Liu, Y.T., K.M. Chang, C.H. Ma, and M. Jayaram. 2016. Replication-dependent and independent mechanisms for the chromosome-coupled persistence of a selfish genome. *Nucleic Acids Res.* 44:8302–8323. http://dx.doi.org/10.1093/nar/gkw694

Marechal, V., A. Dehee, R. Chikhi-Brachet, T. Piolot, M. Coppey-Moisan, and J.C. Nicolas. 1999. Mapping EBNA-1 domains involved in binding to metaphase chromosomes. *J. Virol.* 73:4385–4392.

Matsumura, S., L.M. Persson, L. Wong, and A.C. Wilson. 2010. The latency-associated nuclear antigen interacts with MeCP2 and nucleosomes through separate domains. *J. Virol.* 84:2318–2330. http://dx.doi.org/10.1128/JVI.01097-09

Muralidhar, S., A.M. Pumfery, M. Hassani, M.R. Sadaie, M. Kishishita, J.N. Brady, J. Doniger, P. Medveczky, and L.J. Rosenthal. 1998. Identification of kaposin (open reading frame K12) as a human herpesvirus 8 (Kaposi's sarcoma-associated herpesvirus) transforming gene. *J. Virol.* 72:4980–4988.

Nanbo, A., A. Sugden, and B. Sugden. 2007. The coupling of synthesis and partitioning of EBV's plasmid replicon is revealed in live cells. *EMBO J.* 26:4252–4262. http://dx.doi.org/10.1038/sj.emboj.7601853

Nicklas, R.B. 1997. How cells get the right chromosomes. *Science.* 275:632–637. http://dx.doi.org/10.1126/science.275.5300.632

Norby, K., Y.F. Chiu, and B. Sugden. 2012. Monitoring plasmid replication in live mammalian cells over multiple generations by fluorescence microscopy. *J. Vis. Exp.* Dec 13:e4305.

Ojala, P.M., M. Tiainen, P. Salven, T. Veikkola, E. Castaños-Vélez, R. Sarid, P. Biberfeld, and T.P. Mäkelä. 1999. Kaposi's sarcoma-associated herpesvirus-encoded v-cyclin triggers apoptosis in cells with high levels of cyclin-dependent kinase 6. *Cancer Res.* 59:4984–4989.

Ottinger, M., T. Christalla, K. Nathan, M.M. Brinkmann, A. Viejo-Borbolla, and T.F. Schulz. 2006. Kaposi's sarcoma-associated herpesvirus LANA-1 interacts with the short variant of BRD4 and releases cells from a BRD4- and BRD2/RING3-induced G1 cell cycle arrest. *J. Virol.* 80:10772–10786. http://dx.doi.org/10.1128/JVI.00804-06

Platt, G.M., G.R. Simpson, S. Mittnacht, and T.F. Schulz. 1999. Latent nuclear antigen of Kaposi's sarcoma-associated herpesvirus interacts with RING3, a homolog of the *Drosophila* female sterile homeotic (fsh) gene. *J. Virol.* 73:9789–9795.

Robinett, C.C., A. Straight, G. Li, C. Willhelm, G. Sudlow, A. Murray, and A.S. Belmont. 1996. In vivo localization of DNA sequences and visualization of large-scale chromatin organization using lac operator/repressor recognition. *J. Cell Biol.* 135:1685–1700. http://dx.doi.org/10.1083/jcb.135.6.1685

Russo, J.J., R.A. Bohenzky, M.C. Chien, J. Chen, M. Yan, D. Maddalena, J.P. Parry, D. Peruzzi, I.S. Edelman, Y. Chang, and P.S. Moore. 1996. Nucleotide sequence of the Kaposi sarcoma-associated herpesvirus (HHV8). *Proc. Natl. Acad. Sci. USA.* 93:14862–14867. http://dx.doi.org/10.1073/pnas.93.25.14862

Samols, M.A., R.L. Skalsky, A.M. Maldonado, A. Riva, M.C. Lopez, H.V. Baker, and R. Renne. 2007. Identification of cellular genes targeted by KSHV-encoded microRNAs. *PLoS Pathog.* 3:e65. http://dx.doi.org/10.1371/journal.ppat.0030065

Santag, S., W. Jäger, C.B. Karsten, S. Kati, M. Pietrek, D. Steinemann, G. Sarek, P.M. Ojala, and T.F. Schulz. 2013. Recruitment of the tumour suppressor protein p73 by Kaposi's sarcoma herpesvirus latent nuclear antigen contributes to the survival of primary effusion lymphoma cells. *Oncogene.* 32:3676–3685. http://dx.doi.org/10.1038/onc.2012.385

Schepers, A., M. Ritzi, K. Bousset, E. Kremmer, J.L. Yates, J. Harwood, J.F. Diffley, and W. Hammerschmidt. 2001. Human origin recognition complex binds to the region of the latent origin of DNA replication of Epstein-Barr virus. *EMBO J.* 20:4588–4602. http://dx.doi.org/10.1093/emboj/20.16.4588

Sears, J., M. Ujihara, S. Wong, C. Ott, J. Middeldorp, and A. Aiyar. 2004. The amino terminus of Epstein-Barr virus (EBV) nuclear antigen 1 contains AT hooks that facilitate the replication and partitioning of latent EBV genomes by tethering them to cellular chromosomes. *J. Virol.* 78:11487–11505. http://dx.doi.org/10.1128/JVI.78.21.11487-11505.2004

Shrestha, P., and B. Sugden. 2014. Identification of properties of the Kaposi's sarcoma-associated herpesvirus latent origin of replication that are essential for the efficient establishment and maintenance of intact plasmids. *J. Virol.* 88:8490–8503. http://dx.doi.org/10.1128/JVI.00742-14

Stedman, W., Z. Deng, F. Lu, and P.M. Lieberman. 2004. ORC, MCM, and histone hyperacetylation at the Kaposi's sarcoma-associated herpesvirus latent replication origin. *J. Virol.* 78:12566–12575. http://dx.doi.org/10.1128/JVI.78.22.12566-12575.2004

Stürzl, M., D. Gaus, W.G. Dirks, D. Ganem, and R. Jochmann. 2013. Kaposi's sarcoma-derived cell line SLK is not of endothelial origin, but is a contaminant from a known renal carcinoma cell line. *Int. J. Cancer.* 132:1954–1958. http://dx.doi.org/10.1002/ijc.27849

Sugden, B. 2014. Epstein-Barr virus: The path from association to causality for a ubiquitous human pathogen. *PLoS Biol.* 12:e1001939. http://dx.doi.org/10.1371/journal.pbio.1001939

Thome, M., P. Schneider, K. Hofmann, H. Fickenscher, E. Meinl, F. Neipel, C. Mattmann, K. Burns, J.L. Bodmer, M. Schröter, et al. 1997. Viral FLICE-inhibitory proteins (FLIPs) prevent apoptosis induced by death receptors. *Nature.* 386:517–521. http://dx.doi.org/10.1038/386517a0

van Kuppeveld, F.J., J.T. van der Logt, A.F. Angulo, M.J. van Zoest, W.G. Quint, H.G. Niesters, J.M. Galama, and W.J. Melchers. 1992. Genus- and species-specific identification of mycoplasmas by 16S rRNA amplification. *Appl. Environ. Microbiol.* 58:2606–2615.

Vereide, D.T., and B. Sugden. 2011. Lymphomas differ in their dependence on Epstein-Barr virus. *Blood.* 117:1977–1985. http://dx.doi.org/10.1182/blood-2010-05-285791

Vereide, D.T., E. Seto, Y.F. Chiu, M. Hayes, T. Tagawa, A. Grundhoff, W. Hammerschmidt, and B. Sugden. 2014. Epstein-Barr virus maintains lymphomas via its miRNAs. *Oncogene.* 33:1258–1264. http://dx.doi.org/10.1038/onc.2013.71

Viejo-Borbolla, A., M. Ottinger, E. Brüning, A. Bürger, R. König, E. Kati, J.A. Sheldon, and T.F. Schulz. 2005. Brd2/RING3 interacts with a chromatin-binding domain in the Kaposi's sarcoma-associated herpesvirus latency-associated nuclear antigen 1 (LANA-1) that is required for multiple functions of LANA-1. *J. Virol.* 79:13618–13629. http://dx.doi.org/10.1128/JVI.79.21.13618-13629.2005

Wang, C.Y., and B. Sugden. 2008. Identifying a property of origins of DNA synthesis required to support plasmids stably in human cells. *Proc. Natl. Acad. Sci. USA.* 105:9639–9644. http://dx.doi.org/10.1073/pnas.0801378105

Wies, E., Y. Mori, A. Hahn, E. Kremmer, M. Stürzl, B. Fleckenstein, and F. Neipel. 2008. The viral interferon-regulatory factor-3 is required for the survival of KSHV-infected primary effusion lymphoma cells. *Blood.* 111:320–327. http://dx.doi.org/10.1182/blood-2007-05-092288

Wills, M.R., A.J. Carmichael, and J.G. Sissons. 2002. Vaccines against persistent DNA virus infections. *Br. Med. Bull.* 62:125–138. http://dx.doi.org/10.1093/bmb/62.1.125

Xiao, B., S.C. Verma, Q. Cai, R. Kaul, J. Lu, A. Saha, and E.S. Robertson. 2010. Bub1 and CENP-F can contribute to Kaposi's sarcoma-associated herpesvirus genome persistence by targeting LANA to kinetochores. *J. Virol.* 84:9718–9732. http://dx.doi.org/10.1128/JVI.00713-10

Ye, F.C., F.C. Zhou, S.M. Yoo, J.P. Xie, P.J. Browning, and S.J. Gao. 2004. Disruption of Kaposi's sarcoma-associated herpesvirus latent nuclear antigen leads to abortive episome persistence. *J. Virol.* 78:11121–11129. http://dx.doi.org/10.1128/JVI.78.20.11121-11129.2004

Zhou, F.C., Y.J. Zhang, J.H. Deng, X.P. Wang, H.Y. Pan, E. Hettler, and S.J. Gao. 2002. Efficient infection by a recombinant Kaposi's sarcoma-associated herpesvirus cloned in a bacterial artificial chromosome: Application for genetic analysis. *J. Virol.* 76:6185–6196. http://dx.doi.org/10.1128/JVI.76.12.6185-6196.2002